

## Beam Emittance Growth due to Aberrations in Focusing Lenses

I. Terechkin

### I. Introduction

As beam tracking results in [1] show, after passing through an ideal solenoid-based CH-type focusing lens, beam can acquire some emittance due to spherical aberration. In Fig. 1, three families of sample trajectories are plotted in the vicinity of the rear focal plane. The trajectories (protons,  $E = 2.5$  MeV) were initially parallel to the lens' axis and started at different distances from this axis: 0.15 mm, 5 mm, and 10 mm.

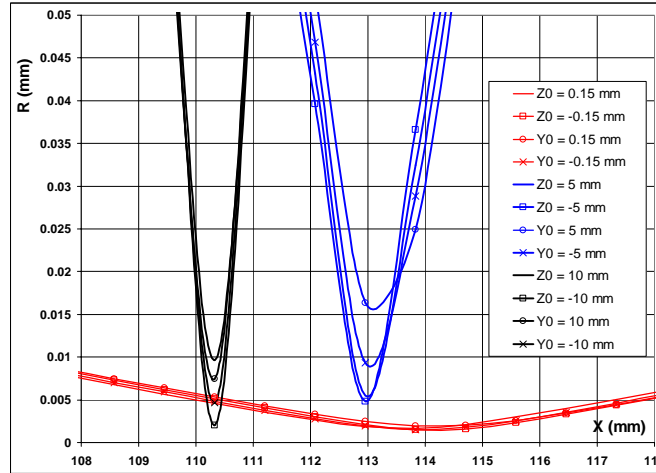


Fig. 1. Projection of sample beam trajectories on the radial plane near the focus plane.

Because the emittance of the incoming subset of sample particles is zero, we can get some information about emittance growth after the lens by analyzing the focal spot. If to choose the longitudinal coordinate  $X = 111$  mm in Fig. 1 as a section to evaluate the emittance, we come to a graph in Fig. 2 that describes the beam quality in terms of the transverse ( $Z, Z'$ ) phase space. Due to spherical symmetry, similar graph in the ( $Y, Y'$ ) phase space is identical. Two curves in the figure correspond to different starting points ( $Y, Z$ ) of the sample trajectories:  $Z = 0, Y = \pm 5$  mm and  $\pm 10$  mm, and  $Y = 0, Z = \pm 5$  mm and  $\pm 10$  mm.

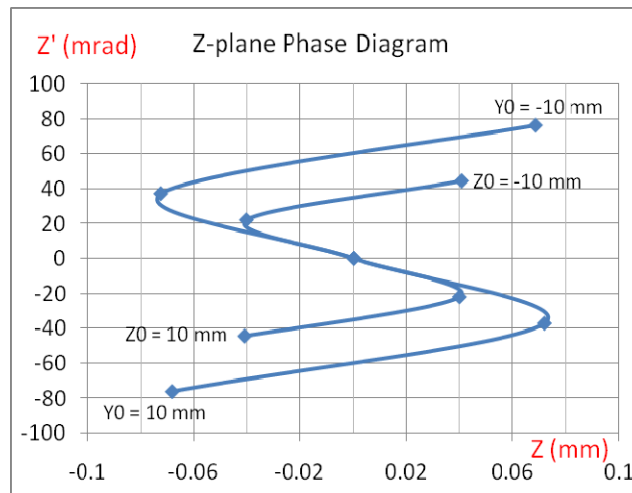


Fig. 2. Phase diagrams in the plane  $X = 111$  mm.

Initially all sample particles were distributed on the phase space diagram in Fig. 2 along the axis  $Z' = 0$  (and  $Y' = 0$ ). The phase space occupied by all the particles in the plane  $X = 111$  mm (rear focal plane) is  $\sim 40$  mm-mrad, which corresponds to the effective normalized emittance of  $\sim 0.93 \pi$  mm-mrad for  $\beta = 0.073$ . Because the expected emittance after RFQ is on the level of  $\sim 0.2 \pi$  mm-mrad, the emittance growth rate of  $\sim 1 \pi$  mm-mrad per lens seems unacceptable. On the other hand, the graph in Fig. 2 also shows that for the initial distances  $Y_0$  and  $Z_0$  smaller than 5 mm, the phase space remains quite small. Expected RMS beam radius in the beam channel of the CH section is  $\sim 2$  mm (in Fig. 3, which is borrowed from [2], the CH section of the linac is at  $D < 15$  m), so there is a hope that for this beam, the increase of the emittance will not be significant. The goal of this note is to investigate this issue for all types of the focusing lenses used in the transport channel of HINS linac front end by using a 3D computational model developed earlier in [1].

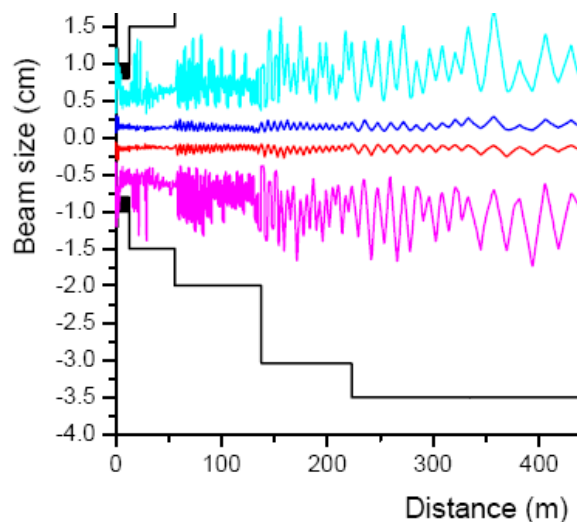


Fig. 3. Beam envelope in the HINS linac.

### I. CH section focusing lens

We will use the model developed in [1] and start several sample traces to represent proton beam (2.5 MeV,  $\beta=0.073$ ) with normalized 2D emittance  $\epsilon_n = 0.4 \pi$  mm-mrad. If to accept the maximum radial size of the beam of 5 mm, the maximum trajectory angle at  $Z = 0$  (or  $Y = 0$ ) is 1.1 mrad. Table 1 provides information about all sample traces, and Fig. 4 shows the phase plane ( $Z, Z'$ ) with coordinates of each sample trajectory in the section  $X = 111$  mm. The ( $Y, Y'$ ) plane is not shown because it is identical to the ( $Z, Z'$ ) plane due to the axial symmetry. Points in red in the graph correspond to red rows in the table. The phase space occupied by the sample particles shows some signs of spherical aberration: sample traces that reach higher radii tend to form some tails. The whole phase space is enclosed by an ellipse that represents an efficient phase space in  $Z-Z'$  plane. The area of the ellipse shown in the graph is 17.6 mm-mrad. Making transformation to the effective normalized emittance, we can write:  $\epsilon_n = 17.6/\pi \cdot 0.073 \approx 0.41 \pi$  mm-mrad. Because the emittance of the sample beam before the lens was  $0.4 \pi$  mm-mrad; a conclusion can be made that if the radial size of the beam passing through the focusing lens of a CH-type is less than 5 mm, emittance growth is not significant.

Table 1

#	Y0 (mm)	Y0' (mrad)	Z0 (mm)	Z0' (mrad)	Z <sub>111</sub> (mm)	Z' <sub>111</sub> (mrad)
1	0	0	0	0	0	0
2	5	0	0	0	0.072	-37
3	-5	0	0	0	-0.072	37
4	0	0	5	0	0.040	-22
5	0	0	-5	0	-0.040	22
6	0	0.55	0	0	0.056	-0.3
7	0	-0.55	0	0	-0.058	0.3
8	0	0	0	0.55	0.033	-0.2
9	0	0	0	-0.55	-0.033	0.2
10			5	0.475	0.068	-22
11			5	-0.475	0.012	-22
12			-5	0.475	-0.015	22
13			-5	-0.475	-0.068	22
14	2.5	1.0			0.142	-19
15	-2.5	-1.0			-0.142	19
16			-2.5	1.0	0.037	11
17			2.5	-1.0	-0.037	-11
18	0	1.2	0	0	0.125	-0.75
19	0	-1.2	0	0	-0.125	0.76

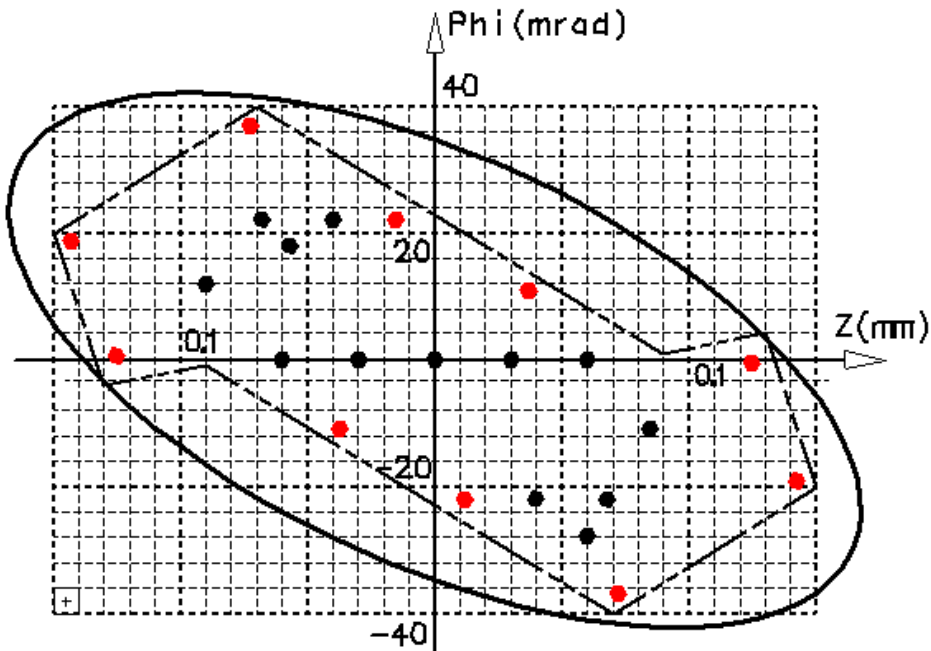


Fig. 4. Z-Z' phase plane with coordinates of representing sample traces through CH-type focusing lens at X = 111 mm (rear focal plane).

## II. SS1 section focusing lens

Similar study of emittance increase should also be made for lenses of solenoid-based lenses of superconducting section SS1 [3]. In this case, the beam energy of 10 MeV was accepted ( $\beta = 0.145$ ), so the beam is more “rigid”. On the other hand, the inner diameter of the coils of these lenses is smaller. Because, as it is seen in Fig. 3, the RMS radius of the beam in the SS1 section ( $15 \text{ m} < Z < 50 \text{ m}$ ) can be more than 10 mm, the trajectories with the initial transverse coordinate of 12.5 mm will be included in the sample trajectory list. At 160 A, which is the nominal current of the lens, it has the next parameters:

Table 2

	R = 0	R = 5 mm	R = 10 mm
$\int B^2 dx \text{ (T}^2\text{-m)}$	3.057	3.074	3.127
$\int B dx \text{ (T-m)}$	0.615	0.615	0.615
F (mm)	273	272	267
Phi (rad)	0.675	0.675	0.675
$B_{\text{eff}}$ (T)	4.97	5.00	5.09
$L_{\text{eff}}$ (mm)	123.6	122.9	120.8

As in the case of the CH lenses, the focusing length  $F$  depends on the distance from the axis, which suggests spherical aberration and possible emittance growth. Polarization rotation angle  $\mathbf{Phi}$ , which depends of the field integral, almost does not change with radius. The initial normalized emittance of  $0.4 \pi \text{ mm-mrad}$  was accepted for the input beam. With  $\beta = 0.145$ , this corresponds to the geometric emittance of  $2.75 \pi \text{ mm-mrad}$ . With the maximum beam radius  $R_m = 12.5 \text{ mm}$ , the maximum trajectory angle in the incident beam  $R'_m = 0.22 \text{ mrad}$ . Several representing particles were launched from the plane  $X_0 = -200 \text{ mm}$ , and their coordinates and trajectory angles were measured after they pass through the lens, at  $X_1 = 200 \text{ mm}$ . Graph in Fig. 5 shows the tracing results on the  $(Z, Z')$  plane. The ellipse shown in the graph encircles the representing points with maximum initial distances from the axis of 10 mm. The area of this ellipse (including not shown symmetric part) is  $\sim 11.3 \text{ mm-mrad}$ , which corresponds to the geometric emittance of  $\sim 3.6 \pi \text{ mm-mrad}$  and normalized emittance of  $\sim 0.5 \pi \text{ mm-mrad}$ . This emittance is a bit higher than what was accepted in the input plane ( $0.4 \pi \text{ mm-mrad}$ ).

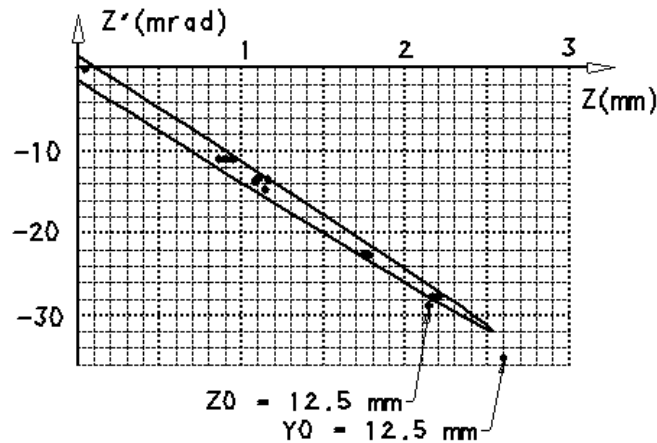


Fig. 5.  $Z$ - $Z'$  phase plane with coordinates of representing sample traces after SS1-type focusing lens at  $X_1 = 200 \text{ mm}$ .

The two points located outside the encircled area correspond to the initial position of sample particles at the edge of the input phase space:  $Z_0 = 12.5$  mm and  $Y_0 = 12.5$  mm. If to take these particles into account, we ought to recognize significant growth of the emittance due to aberrations in the lens. As the particle energy increases, the emittance growth after lenses will become smaller. It is important to keep transverse size of the beam at the input to the SS1 section of the linac reasonably small at least in the initial section of the cryomodule.

### III. SS0 section focusing lens

Having in mind this result, it is important to understand potential problem we can have in the front end of the PX linac. In this linac, the first (low energy) section is made superconducting, with solenoid focusing. This brings the requirement of having low magnetic field on the walls of accelerating (superconducting) cavities. First approach to the focusing lens design is similar to that of the SS1 section (which was proved to have low fringe magnetic field [4]). Because the energy in this section is lower than in the SS1 section, the required focusing strength of the lens is lower than in the SS1 section. While making the first attempt to approach the design, the needed strength of  $1.8 \text{ T}^2 \cdot \text{m}$  was accepted as it was for the room temperature (CH) section of the HINS linac. Dipole corrector assembly with thin radial profile was accepted for the SS0 lens design, as it was made in the SS1\_PP lens. Each SS0 lens will be also equipped with a beam position monitor, similar to those designed for installation in the RT section of the HINS linac. The concept of the SS0 section lens design is shown in Fig. 6. Superconducting strand and the number of turns in each coil of the lens were chosen identical to what was used in the CH-T2 focusing lenses, but the inner diameter of the windings is different, and LHe vessel design was slightly modified to save longitudinal space.

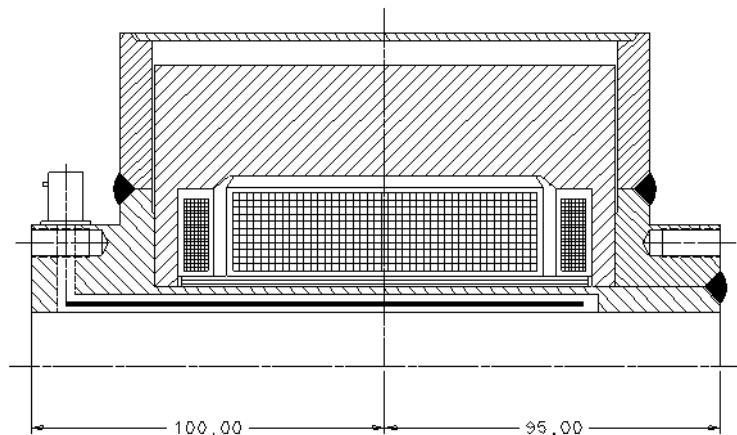


Fig. 6. SS0 lens design concept

Smaller inner diameter of the lens coils windings was accepted to relax possible magnetic shielding problems; nevertheless, verification modeling showed that 10 mT fringe field requirement can be satisfied only if two layers of magnetic shielding is used. Because the inner diameter of the coils in the SS0 lens is smaller than it was in the CH lens (see part I of this note), there is a concern that this can result in unacceptable increase of the emittance in this section. If this is the case, the lens design must be modified to increase the inner diameter and to find a new solution for the magnetic field

shielding. To address this concern, a 3D model was generated to make the tracing studies (Fig. 7).

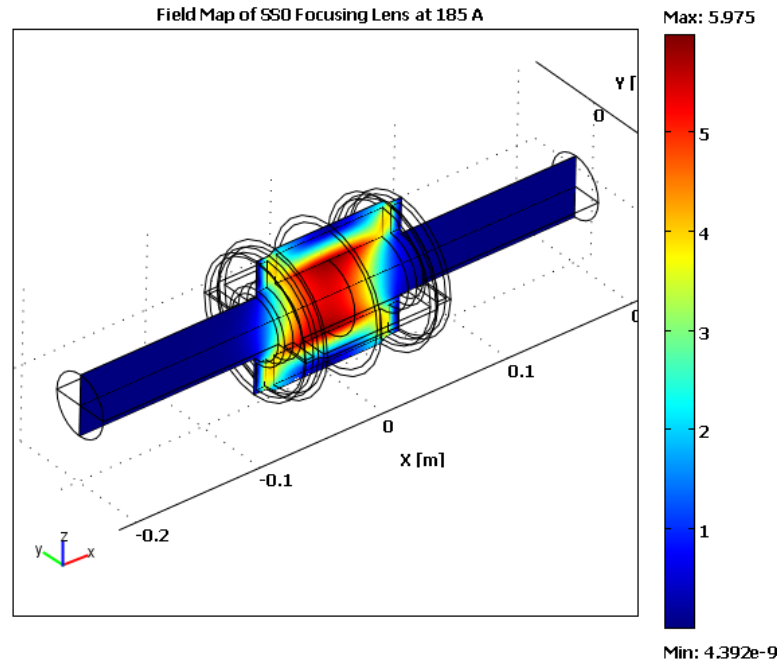


Fig. 7. 3D model of the SS0 section focusing lens with a color map of the magnetic field in the central cross section.

The energy of the particles (protons) was 2.5 MeV ( $\beta = 0.073$ ), like it was for the CH-type lenses. The initial normalized emittance was accepted on the level 0.4 mm-mrad with  $R_m = 7.5$  mm. Tracing was also made for particles with  $R_m = 10$  mm and 12.5 mm. Main results of this study are summarized in Table 3 and visualized in Fig. 8, where a representing ellipse is built for the particles within  $R_m = 7.5$  mm for the cross-section in the vicinity of the rear focal plane  $Z_1 = 126$  mm. An area encircled by this ellipse (including not shown, symmetrical part) is 15.2 mm-mrad. This area corresponds to the normalized emittance  $\epsilon_n = 0.35 \pi$  mm-mrad, which is in a good agreement with the initial emittance of  $0.4 \pi$  mm-mrad.

As the maximum initial distance of the sample particles from the axis increases, the imprint of the particles on the phase space at the exit of the lens goes far beyond this representing ellipse. With  $R_m = 10$  mm, the representing ellipse corresponding to this maximum radius gives  $\epsilon_n = 0.75 \pi$  mm-mrad, which is almost two times higher than the initial emittance. For  $R_m = 12.5$  mm, the normalized emittance at  $Z_1 = 126$  mm becomes  $3.5 \pi$  mm-mrad.

So, to avoid significant emittance growth, the beam radial size must be kept below 7.5 mm within SS0 section.

Table 3

	$R_0$ (mm)	$R'_0$ (mrad)	$Z_{126\text{mm}}$ (mm)	$Z'_{126\text{mm}}$ (mrad)
1	5	0	0.054	-31.3
2			0.035	-22.5
3			0.044	-22.4
4			-0.057	31.2
5	7.5	0	0.023	-47.4
6			0.023	-33.8
7			0.018	-33.8
8			-0.026	47.4
9	5	0.546	0.08	-22.6
10			-0.11	31.5
11			0.005	-22.5
12			-0.002	30.9
13			0.1	-22.6
14			-0.015	31.0
15			-0.013	-22.1
16			-0.098	31.4
17	10	0	-0.075	-64.1
18			-0.057	-45.6
19			-0.05	-10.8
20			-0.088	15.4
21	12.5	0	-0.265	-81.7
22			-0.205	-57.7
23			-0.188	-57.6
24			-0.286	81.7

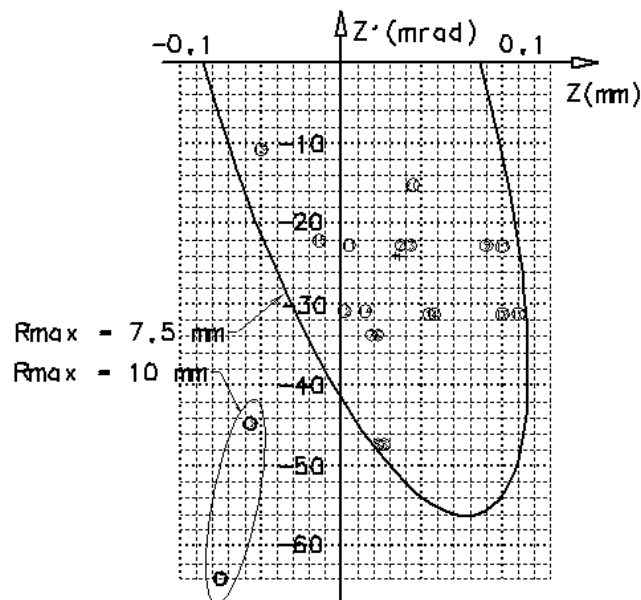


Fig. 8.  $Z-Z'$  phase plane with coordinates of representing sample traces after SS0-type focusing lens at  $X = 126$  mm (rear focal plane).

#### IV. Conclusion

This study was conducted to understand what restrictions should be imposed on the beam radial size if solenoid-based focusing lenses are used in transport sections of a proton linac. 3D computational models were developed and beam tracing analysis was made for the CH section and SS1 section lenses of the HINS linac and for the SS0 section of a PX linac front end. The CH lens will not increase the beam emittance if the beam size is kept within the limits designed by the beam transport design. The SS1 lens works well if the beam radius is below 10 mm. For the SS0 lens, the obtained results indicate that the beam radius must be kept below 7.5 mm to prevent emittance growth. Partial controversy exists if CH and SS0 lenses are compared: SS0 lenses can tolerate larger beam radius, although having smaller inner radius of the windings. Most probably, this resulted from having significantly finer mesh size in the case of the SS0 lens. Fig. 1 shows radial distance to the axis from different sample traces; these distances should be identical for the traces of the same family with equal initial distance from the axis. Numerical noise due to the final size of the mesh explains the difference.

The lenses that were studied were "ideal" in the sense that they were made in accordance with the magnetic design (zero tolerances). Impact of imperfectness in fabrication and alignment will be studied later.

#### References:

1. J. DiMarco, M. Tartaglia, and I. Terechkine, "Optical Properties of a CH-Type focusing Lens", FNAL TD note TD-10-004.
2. P. Ostroumov, "Design Concept for a Pulsed Multi-GeV  $H^-$  linac", <http://projectx-docdb.fnal.gov/cgi-bin/RetrieveFile?docid=430&version=1&filename=HINS%20linac.pdf>
3. G. Gavis, et al, "Pre-Production Solenoid for SS1 Section of HINS Linac", TD-09-010, FNAL, 2009.
4. G. Davis, et al, "Magnetic Shielding of Solenoid-Based Focusing Lenses for Superconducting Sections of HINS Linac" TD-09-029, FNAL, 2009